HOSTED BY

ELSEVIER

Available online at www.sciencedirect.com

ScienceDirect

Journal of Magnesium and Alloys 3 (2015) 302–308
www.elsevier.com/journals/journal-of-magnesium-and-alloys/2213-9567

Full Length Article

Reducing the tension–compression yield asymmetry of extruded Mg–Zn–Ca alloy via equal channel angular pressing

L.B. Tong [a], M.Y. Zheng [b], S. Kamado [c], D.P. Zhang [a], J. Meng [a], L.R. Cheng [a,*], H.J. Zhang [a,**]

[a] *State Key Laboratory of Rare Earth Resources Utilization, Changchun Institute of Applied Chemistry, Chinese Academy of Sciences, Changchun 130022, China*

[b] *School of Materials Science and Engineering, Harbin Institute of Technology, Harbin 150001, China*

[c] *Department of Mechanical Engineering, Nagaoka University of Technology, Nagaoka 940-2188, Japan*

Received 17 July 2015; revised 11 August 2015; accepted 25 August 2015

Available online 2 December 2015

Abstract

The influence of equal channel angular pressing on the tension–compression yield asymmetry of extruded Mg–5.3 Zn–0.6 Ca (weight percent) alloy has been investigated. The microstructure was obviously refined by the large strain during the equal channel angular pressing, accompanied with very fine $Ca_2Mg_6Zn_3$ phases with average diameter of 70 nm. The weak tension–compression yield asymmetry after equal channel angular pressing is mainly attributed to the reduced volume fraction of extension twinning during the compression, because the slope (k) of twinning in Hall–Petch relationship is higher than that of dislocation slip, and the twinning deformation is difficult to take place with decreasing grain size. The basal slip is more active in the alloy after equal channel angular pressing, due to the non-basal texture components, which hinders the twinning activation and reduces the yield asymmetry. Furthermore, the presence of fine precipitate restricts the twinning activation, which also contributes to the reduction of yield asymmetry.

Keywords: Mg–Zn–Ca alloy; Yield asymmetry; Equal channel angular pressing; Twinning; Precipitates

1. Introduction

Mg and its alloys are the least of all metals being used in practice for structural materials [1], but the low strength and poor ductility of the Mg alloys prepared by gravity casting limit their industrial applications. The conventional thermo-mechanical processing, such as extrusion, rolling and forging, can remarkably improve the mechanical properties of cast Mg alloys [2–4]. In contrast to cubic metals, the undesirable yield strength asymmetry of wrought Mg alloys during the compression and tension usually appears, due to the low-asymmetry of hexagonal close packing (HCP) structure [5,6]. Recent reports have confirmed that when the wrought Mg alloys with the conventional basal texture are loaded along the extrusion or rolling direction, the twinning activation results in tension–compression yield asymmetry [7,8]. The twinning is strongly dependent on grain size [9], thus the role of the grain refinement on the yield asymmetry of Mg alloy is of particular interest. Moreover, fine secondary phase particles also contribute to the asymmetry of Mg alloys. Jain et al. [10] reported that the presence of dense $Mg_{17}Al_{12}$ precipitates in aged Mg–8 Al–0.5 Zn alloy could reduce the tension–compression yield asymmetry, through hindering the twin growth.

Recently, the ternary Mg–Zn–Ca alloys have attracted much attention due to their low cost and superior mechanical properties; Zn and Ca, together with Mg, can obtain a stable intermetallic compound $Ca_2Mg_6Zn_3$ with high hardness and good creep resistance [11,12]. During the last decade, equal channel angular pressing (ECAP) is a well-known method of fabricating ultra-fine grained (UFG) metals and alloys, through introducing large strain [13]. Previous studies indicated that the grain refinement and texture evolution occurred during the ECAP, the conventional basal-type texture of wrought Mg alloy was remarkably weakened, and non-basal texture components could

* Corresponding author. State Key Laboratory of Rare Earth Resources Utilization, Changchun Institute of Applied Chemistry, Chinese Academy of Sciences, Changchun 130022, China. Tel.: +86 431 85262414; fax: +86 431 85685653.

E-mail address: lrcheng@ciac.ac.cn (L.R. Cheng).

** Corresponding author. State Key Laboratory of Rare Earth Resources Utilization, Changchun Institute of Applied Chemistry, Chinese Academy of Sciences, Changchun 130022, China. Tel.: +86 431 85262127; fax: +86 431 85698041.

E-mail address: hongjie@ciac.ac.cn (H.J. Zhang).

http://dx.doi.org/10.1016/j.jma.2015.08.007

be formed as well [14–17], which might influence the yield asymmetry. To date, the systematic investigations of the influence of the ECAP processing on the yield asymmetry of wrought Mg–Zn–Ca alloys have not been reported yet, and the corresponding mechanisms remain unclear. The purpose of this work is to investigate the influence of microstructural and texture evolution from ECAP on the tensile and compressive yield behaviors of extruded Mg–Zn–Ca alloy, and give an insight into the mechanism of room-temperature yield asymmetry.

2. Materials and methods

The Mg–5.3 Zn–0.6 Ca (wt.%) alloy was prepared by gravity casting under an SF_6 and CO_2 protective atmosphere; the melts were held at 700 °C for 10 min and then cast into a steel mold. The cast ingot was homogenized at 460 °C for 8 h, and then extruded to a rod bar (with the diameter of 20 mm) at 300 °C with extrusion ratio of 10:1. The ECAP billets, with cross-sectional dimensions of 10×10 mm^2 and a length of 65 mm, were machined from the extruded bars along the extrusion direction (ED). The ECAP was carried out at 250 °C for four passes (route Bc [13,15], a total strain of $\varepsilon \approx 4.2$), using a designed die with internal and external angle of $\Phi = 90°$ and $\psi = 37°$, respectively.

The microstructure was observed along the longitudinal section (parallel to the normal and extrusion or ECAP direction, ND and ED) using an Olympus optical microscope (OM), a JEOL FESEM JSM-7000F scanning electron microscopy and a Philips Tecnai-F20 transmission electron microscope (TEM), and the quantitative analysis of microstructure was calculated using the software of Image-Pro Plus 5.0. Electron backscattered diffraction (EBSD) analysis was performed using FESEM equipped with TSL MSC-2200. The global textures of Mg–Zn–Ca alloys were measured using the neutron diffractometer TEX-2. Dog-bone shaped tensile specimens with a dimension of $15 \times 6 \times 2$ mm^3, and rod shaped compressive specimens with a diameter of 8 mm and a length of 12 mm, were cut from the longitudinal section of the extruded and ECAPed bars. The tensile and compressive tests were conducted on Instron 5569 machine with a strain rate of 1.67×10^{-3} s^{-1} at room temperature.

3. Results and discussion

3.1. As-received microstructure and texture

Fig. 1 shows the microstructures of the as-extruded and as-ECAPed alloys. The as-extruded alloy exhibited an equiaxed grain structure, with average grain size of 4.0 μm (Fig. 1a). The dynamic recrystallization process during ECAP results in an obvious grain refinement, and the average grain size decreases to 1.0 μm, representing an ultra-fine grained structure (Fig. 1b). Moreover, the stringer of secondary phases (white contrast), which has been proved as $Ca_2Mg_6Zn_3$ in our previous study [18], is elongated along the ED in the as-extruded alloy. In contrast, a large number of finer spherical particles can be observed in the as-ECAPed alloy, which would hinder the grain growth and promote the grain refinement.

In order to further investigate the detailed constitution and distribution of secondary phases, Fig. 2 shows the TEM micrographs of the Mg–Zn–Ca alloys. The coarse $Ca_2Mg_6Zn_3$ phases break into finer particles in the as-extruded alloy, with the average diameter of ~500 nm, and very few finer precipitate particles (~100 nm) can be also observed (shown by dashed lines in Fig. 2a). There are a large number of finer particles with diameter of ~70 nm in the as-ECAPed alloy (black arrows in Fig. 2b), which is related to the precipitation process, since the ECAP temperature in this study is about the same as the aging temperature. Fig. 2c and d shows the high-resolution electron microscopy (HREM) of the interfaces between the precipitates and α-Mg matrix. These finer precipitates are also proved as $Ca_2Mg_6Zn_3$ phases; the orientation relationship between the $Ca_2Mg_6Zn_3$ precipitates and α-Mg matrix is $(0\bar{1}11)_{\alpha-Mg} // (\bar{3}302)_{Ca_2Mg_6Zn_3}$ $[11\bar{2}3]_{\alpha-Mg} // [20\bar{2}3]_{Ca_2Mg_6Zn_3}$ in both as-extruded and as-ECAPed alloys, while the density of precipitates is dramatically increased after ECAP. The interplanar spacing of $(0\bar{1}11)$ in α-Mg and $(\bar{3}302)$ in $Ca_2Mg_6Zn_3$ phase is calculated as 0.2453 and 0.2456 nm, respectively, and thus the $Ca_2Mg_6Zn_3$ phases are preferably precipitated along the defined habit plane, in order to minimize the lattice mismatch. The volume fraction of $Ca_2Mg_6Zn_3$ precipitates in the as-extruded alloy is below 1.0%, while a large quantity of $Ca_2Mg_6Zn_3$ phases can be precipitated during the repeating ECAP processing. Furthermore, the $Ca_2Mg_6Zn_3$

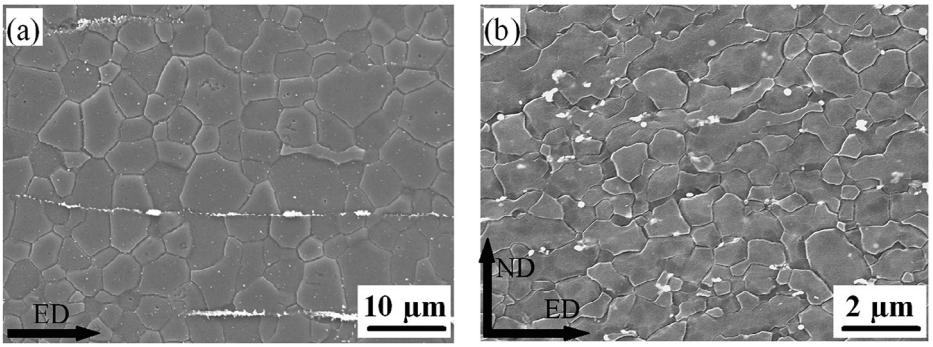

Fig. 1. SEM micrographs of the (a) as-extruded and (b) as-ECAPed Mg–Zn–Ca alloy.

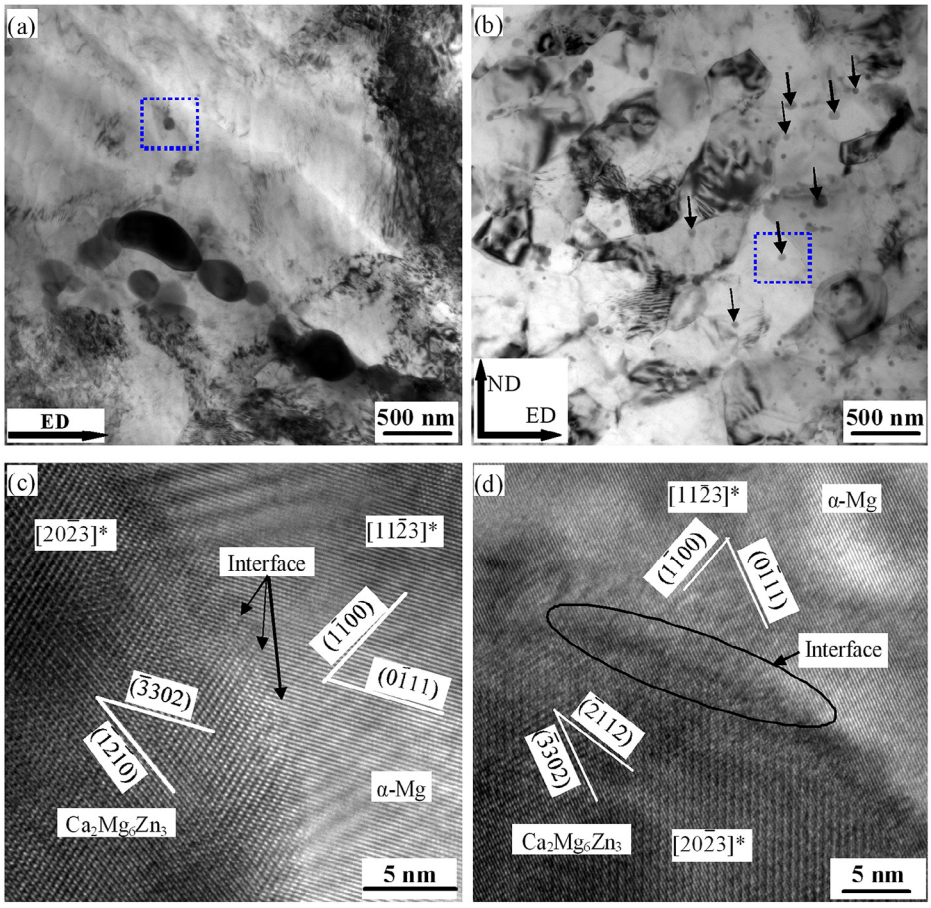

Fig. 2. TEM analysis of (a) as-extruded and (b) as-ECAPed alloy, (c) and (d) HREM of dashed lined area in (a) and (b).

precipitates of the as-ECAPed alloy are much finer than that of as-extruded alloy, due to the lower ECAP temperature.

Fig. 3 shows the texture of the as-extruded and as-ECAPed Mg–Zn–Ca alloys. The as-extruded alloy represents a typical basal texture, with most {0001} planes parallel to ED (Fig. 3a). After ECAP for 4 passes, most of {0001} planes have been inclined ~45° to both ED and ND, and another weak texture component with {0001} plane parallel to ED can also been observed. The texture evolution during ECAP processing is influenced by the strain path; the specimen is rotated around ED in route Bc, which induced the derivation of the conventional basal texture in the as-extruded alloy [18]. The different textures play an important role on the mechanical properties and deformation behaviors of the as-extruded and as-ECAPed alloys, which will be discussed in the following section.

3.2. Tensile–compressive yield asymmetry

Fig. 4 shows the tensile and compressive curves of the as-extruded and as-ECAPed Mg–Zn–Ca alloys at ambient temperature. An obvious yield asymmetry can be observed in the as-extruded alloy (Fig. 4a), and the ratio between compressive yield stress (CYS, ~ 138 MPa) and tensile yield stress (TYS, ~ 178 MPa), corresponding to a 0.2% offset, is calculated as 0.8. Furthermore, the as-extruded alloy presents the different work hardening (WH) behaviors during the tensile and compressive tests. An obvious yield plateau can be observed when the compressive stress is reached above 150 MPa; the WH rate is much lower in this low strain area. With strain proceeding, the compressive curve becomes "concave", the WH rate is remarkably enhanced, and ultimate compressive stress (UCS) is increased to 447 MPa. These "concave" curves have also been observed previously in the extruded Mg alloys, which resulted from $\{10\bar{1}2\}$ extension twinning [19]. In contrast, the tensile curve is "convex", representing a lower WH rate, and the ultimate tensile stress (UTS) is 276 MPa.

After ECAP processing, the tensile and compressive curves are almost the same at the initial stage of deformation (lower strain region); the CYS and TYS are increased to 188 MPa and 180 MPa, respectively, compared with that of the as-extruded alloy; and the CYS/TYS is increased to ~1.0 (Fig. 4b). The work hardening rate is more intensive during the compression, resulting in a higher UCS of 322 MPa, while the elongation is dramatically decreased to 7.1%. The tensile curve is "convex" during the entire plastic deformation, and the compressive curve represents "concave" shape, especially after 3% strain, but the slope is much lower than that of the as-extruded alloy. The ECAP processing can effectively reduce the tension–compression asymmetry of as-extruded Mg–Zn–Ca alloy,

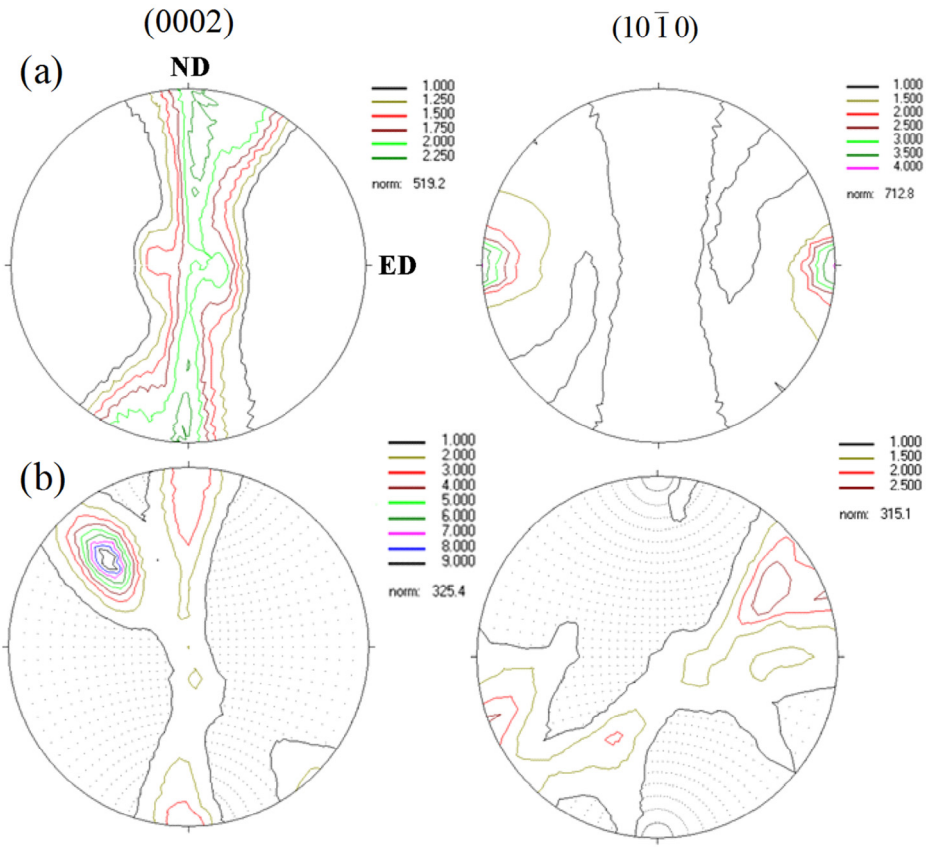

Fig. 3. Pole figures of (a) the as-extruded and (b) as-ECAPed Mg–Zn–Ca alloys.

which is related to the corresponding microstructure and texture evolution.

3.3. Post-deformation microstructure

It can be assumed that the different deformation mechanisms during the initial stage of tensile and compressive tests result in the yield asymmetry, and the detailed microstructural evolution during the tensile and compressive tests is shown in Fig. 5. The microstructure of the as-extruded alloy after 2% tensile strain (Fig. 5a) is almost the same as that of the as-received alloy (Fig. 1a), the twinning deformation does not occur, the dislocation slip dominates the initial stage of tensile deformation, and the TYS is mainly influenced by grain size and texture. Conversely, a large number of twins can be observed in the specimen compressed to 2% (Fig. 5b), and the low angle grain boundaries (LAGBs, ≤15°) are also present within the original grains (Fig. 5c), which reveal that the initial stage of deformation is controlled by both twinning and dislocation slip. Fig. 5d shows the misorientation angle distribution of the as-extruded alloy compressed to 2%; the intensive peak of 85~90° is related to the $\{10\bar{1}2\}$ extension twins. According to the geometric condition, the extension twinning occurs during the tension parallel to the *c*-axis or compression perpendicular to *c*-axis and results in the elongation of Mg alloys along *c*-axis.

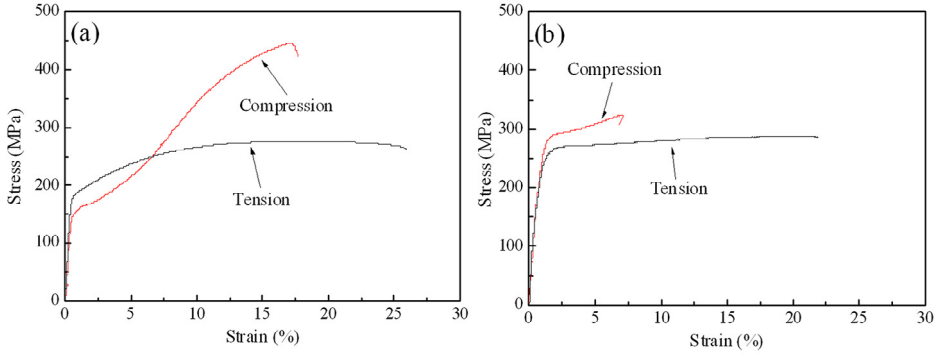

Fig. 4. Room-temperature tensile and compressive curves of the (a) as-extruded and (b) as-ECAPed Mg–Zn–Ca alloys.

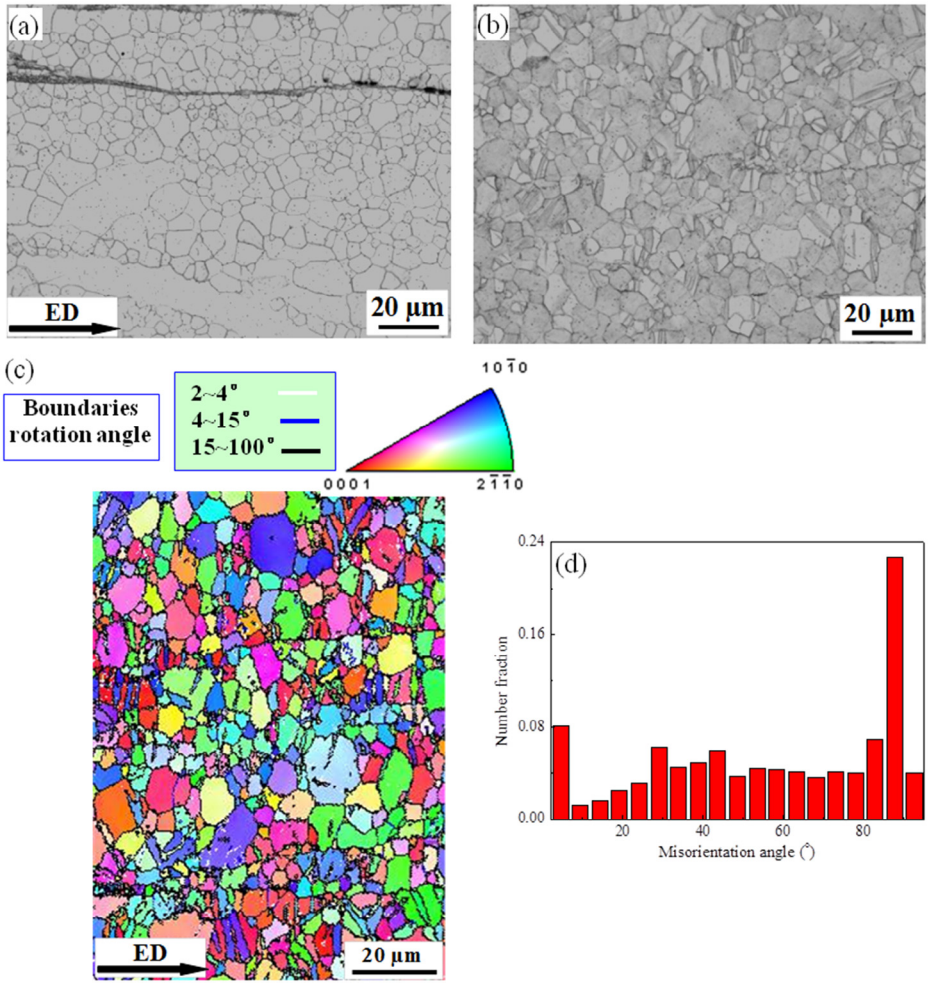

Fig. 5. Optical microstructure of the as-extruded alloy with (a) 2% tensile strain and (b) 2% compressive strain, (c) orientation imaging microscopy and (d) misorientation angle distribution of the as-extruded alloy with 2% compressive strain.

Therefore, for the as-extruded Mg–Zn–Ca alloy with basal texture (Fig. 3a), the twinning can only occur during the compression along the ED.

Fig. 6 shows the microstructure of the as-ECAPed alloy deformed to 2%. Twinning deformation cannot be observed during both the tension and compression, and the grain size of α-Mg, the size and distribution of the secondary phase are almost the same with that of Fig. 1b. Therefore, the twinning can hardly occur in the as-ECAPed alloy, which is related to its UFG structure. It was reported that the Hall–Petch slope of twinning was greater than that of dislocation slip [9,19,20]; with decreasing grain size, the increase rate of critical resolved

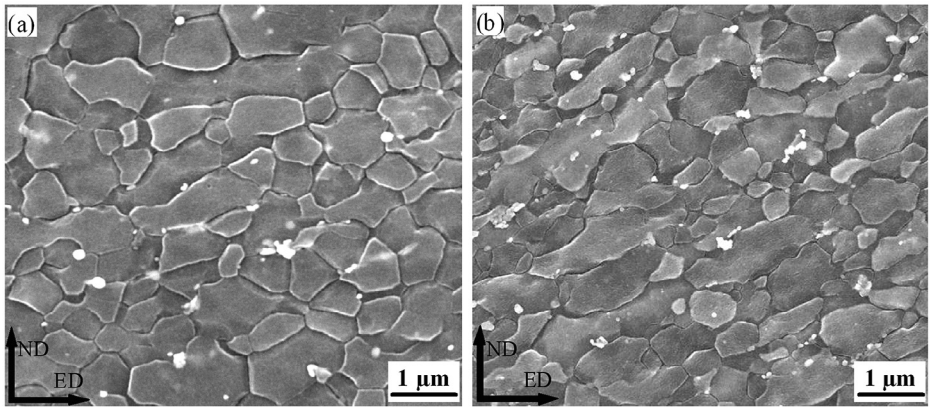

Fig. 6. SEM micrographs of as-ECAPed alloy deformed to 2% during (a) tension, (b) compression.

shear stress (CRSS) for twinning was much higher. Therefore, the twinning activation is more difficult than dislocation slip in fine-grained Mg alloys.

For the as-extruded alloy, the flow stress for twinning activation is much lower than that of dislocation slip due to the intensive basal texture, and the twinning process cannot increase the dislocation density, resulting in a low WH rate. With further straining, a large number of twinning boundaries have been formed, which introduces the additional barriers to dislocation movement [19], and thus the WH rate is remarkably increased, representing a "concave" compressive curve, and the detailed contribution of twinning activation to the yield stress of Mg–Zn–Ca alloys will be discussed in the following section.

3.4. Deformation mechanism

Based on the above analysis, the deformation mechanism of the as-extruded and as-ECAPed Mg–Zn–Ca alloys has been clarified. The tension–compression yield asymmetry resulted from $\{10\bar{1}2\}$ twinning, which is mainly influenced by three aspects: grain size, crystallographic texture and precipitation.

In the current study, the compressive deformation of the as-extruded alloy is mainly controlled by twinning and basal slip; using the law of mixture, the yield stress can be represented as [21]:

$$\sigma_{YS} = (1 - X_{TW})\sigma_{basal} + X_{TW}\sigma_{TW} \quad (1)$$

where X_{TW} is the volume fraction of grains within which the twinning takes place, σ_{YS} is the yield stress, and the σ_{basal} and σ_{TW} are the stress in the grains undergoing basal slip and twinning, respectively. The twinning activation is not observed in the as-extruded alloy during the tensile test, and thus the σ_{YS} is mainly attributed to the basal slip; the σ_{basal} is ~178 MPa. The value of X_{TW} is measured as 37% in the specimen compressed to 2%, and the corresponding σ_{TW} is calculated as ~70 MPa.

The yield stress for twinning (σ_{TW}) is determined by the CRSS (τ_{TW}) and orientation factor (Schmid factor, SF, m_{TW}). The crystallographic texture of Mg alloy determines the orientation relationship between each grain and applied stress, and thus the conventional Hall–Petch relationship can be modified as Equation(2), which is also applied when the yielding behavior is controlled largely by dislocation slip.

$$\sigma_{TW(basal)} = \frac{\tau_{TW(basal)}}{m_{TW(basal)}} + k_{TW(basal)}d^{-1/2} \quad (2)$$

The conventional basal fiber texture has been reported in the extruded Mg–Zn–Ca alloy [22]; the corresponding value of average Schmid factor ($\bar{m}_{basal}$) for basal slip is only 0.23, while the value of $\bar{m}_{TW}$ is calculated as 0.43 from EBSD analysis. According to the previous study [23], the intensive basal texture results in the groups of grains with similar orientation, facilitating the propagation of basal slip across the grain boundaries, and thus the value of k is ~180 MPa. The yielding behavior of the as-extruded alloy is mainly controlled by basal slip system during the initial stage of tension, and the CRSS of basal slip (τ_{basal}) is calculated as 21 MPa, which is similar to the published value of AZ31 alloy [24].

It was reported that the value of τ_{TW} was ~30 MPa [25], assuming that the transition from twinning to dislocation slip dominated deformation occurs when the value of σ_{TW} is twice as high as σ_{basal} in the as-ECAPed alloy (the value of $\bar{m}_{basal}$ and $\bar{m}_{TW}$ is calculated as 0.28 and 0.39 by EBSD analysis), and the corresponding value of k_{TW} is calculated as 433 MPaμm$^{1/2}$ in this study according to Equation (2), which is much higher than that of dislocation slip in Mg alloy (150~350 MPa) [26–28]. The higher Hall–Petch slope (k_{TW}) results in the effect of grain size on twinning deformation is more obvious than dislocation slip, which hinders the twinning activation, and thus the dislocation slip is the main mechanism in the as-ECAPed alloy with a UFG structure.

Furthermore, the crystallographic texture plays an important role on the yield asymmetry. Yin et al. [25] reported that when the load direction was 45° tilting to extrusion direction, the twined grain fraction after tension and compression was almost the same in extruded AZ31 alloy with characteristic basal texture, which reduced the yield asymmetry. Therefore, the volume fraction of extension twins is related to the crystallographic texture. In the current study, most of {0002} planes in the as-ECAPed alloy were inclined about 36° to ED [22]; the Schmid factor for extension twinning is remarkably decreased, and thus the twinning activation is restricted during tension or compression. On the other hand, the basal slip is favorably activated and dominates the initial stage of deformation, because this non-basal texture increases the Schmid factor for basal slip, which also reduces the yield asymmetry.

Considering the contribution from the precipitations based on the Orowan strengthening mechanism [29], the τ_{TW} should be modified by:

$$\tau_{TW} = \tau_0^{TW} + \frac{Gb}{2\pi\lambda\sqrt{1-\gamma}}\ln\frac{d_P}{r_0} \quad (3)$$

where τ_0^{TW} is the CRSS of extension twinning regardless of the precipitation, G is shear modulus (19,200–8.6T) MPa, b is Burgers vector (3.21×10^{-10} m for Mg), λ and d_P are the effective planar spacing and the mean planar diameter of precipitations, respectively, and r_0 is the core radius of dislocations; it is convenient to assume $r_0 = b$. The contribution of precipitation to τ_{TW} can be calculated as ≤0.005 (the volume fraction of precipitate is very low, and thus the value of λ is very large) and ~3.7 MPa in the as-extruded and as-ECAPed alloys, respectively. Therefore, the precipitation of fine $Ca_2Mg_6Zn_3$ phase also restricts the activation of extension twinning and reduces the yield asymmetry of the as-ECAPed alloy (even if this contribution is much lower than the grain refinement), which is consistent with the previous study [10]. Although the effect of $Ca_2Mg_6Zn_3$ precipitation on the twinning activation can be represented quantitatively, the Orowan mechanism for twinning activation, especially the effect of morphology and orientation of precipitates on the CRSS for twinning and the rate of twinning propagation, is still unclear, and more details are needed for further study.

4. Conclusions

1. The coarse $Ca_2Mg_6Zn_3$ phases break into finer particles after extrusion, and much finer $Ca_2Mg_6Zn_3$ phases of ~70 nm precipitate along the defined habit plane during the repeated ECAP processing.
2. The grain refinement and higher Hall–Petch slope restrict the activation of extension twinning in the as-ECAPed alloy, and the compression–tension yield asymmetry is remarkably reduced; the value of CYS/TYS is nearly 1.0.
3. The texture evolution during ECAP decreases the Schmid factor for twinning, and the fine precipitations increase the CRSS of twinning activation, which also contribute to the reduction of yield asymmetry.

Acknowledgements

The authors wish to highly acknowledge Prof. L.M. Wang of Changchun Institute of Applied Chemistry, Chinese Academy of Sciences, for his valuable suggestions and discussions. Thanks to the financial aid from the National Science & Technology Pillar Program (Grant No. 2012BAE01B04), the National Natural Science Foundation of China (Grant No. 51401200), the Natural Science Foundation of Jilin Province (Grant No. 20140520099JH).

References

[1] B.L. Mordike, T. Ebert, Mater. Sci. Eng. A Struct. Mater. 302 (2001) 37–45.
[2] T. Homma, N. Kunito, S. Kamado, Scr. Mater. 61 (2009) 644–647.
[3] X. Li, T. Al-Samman, G. Gottstein, Mater. Des. 32 (2011) 4385–4393.
[4] S.K. Panigrahi, W. Yuan, R.S. Mishra, R. DeLorme, B. Davis, R.A. Howell, et al., Mater. Sci. Eng. A Struct. Mater. 530 (2011) 28–35.
[5] E.A. Ball, P.B. Prangnell, Scr. Mater. 31 (1994) 111–116.
[6] Z. Zachariah, S.S.V. Tatiparti, S.K. Mishra, N. Ramakrishnan, U. Ramamurty, Mater. Sci. Eng. A Struct. Mater. 572 (2013) 8–18.
[7] X.Y. Lou, M. Li, R.K. Boger, S.R. Agnew, R.H. Wagoner, Int. J. Plast. 23 (2007) 44–86.
[8] P. Klimanek, A. Pötzsch, Mater. Sci. Eng. A Struct. Mater. 324 (2002) 145–150.
[9] M.R. Barnett, Scr. Mater. 59 (2008) 696–698.
[10] J. Jain, W.J. Poole, C.W. Sinclair, M.A. Gharghouri, Scr. Mater. 62 (2010) 301–304.
[11] T.V. Larionova, W.W. Park, B.S. You, Scr. Mater. 45 (2001) 7–12.
[12] J.C. Oh, T. Ohkubo, T. Mukai, K. Hono, Scr. Mater. 53 (2005) 675–679.
[13] R.Z. Valiev, T.G. Langdon, Prog. Mater. Sci. 51 (2006) 881–981.
[14] S.R. Agnew, P. Mehrotra, T.M. Lillo, G.M. Stoica, P.K. Liaw, Acta Mater. 53 (2005) 3135–3146.
[15] W.M. Gan, M.Y. Zheng, H. Chang, X.J. Wang, X.G. Qiao, K. Wu, et al., J. Alloys Compd. 470 (2009) 256–262.
[16] F. Akbaripanah, F. Fereshteh-Saniee, R. Mahmudi, H.K. Kim, Mater. Des. 43 (2013) 31–39.
[17] R. Jahadi, M. Sedighi, H. Jahed, Mater. Sci. Eng. A Struct. Mater. 593 (2014) 178–184.
[18] L.B. Tong, M.Y. Zheng, H. Chang, X.S. Hu, K. Wu, S.W. Xu, et al., Mater. Sci. Eng. A Struct. Mater. 523 (2009) 289–294.
[19] M.R. Barnett, Z. Keshavarz, A.G. Beer, D. Atwell, Acta Mater. 52 (2004) 5093–5103.
[20] Q. Yu, Z.W. Shan, J. Li, X.X. Huang, L. Xiao, J. Sun, et al., Nature 463 (2010) 335–338.
[21] M.R. Barnett, C.H.J. Davies, X. Ma, Scr. Mater. 52 (2005) 627–632.
[22] L.B. Tong, M.Y. Zheng, X.S. Hu, K. Wu, S.W. Xu, S. Kamado, et al., Mater. Sci. Eng. A Struct. Mater. 527 (2010) 4250–4256.
[23] C.H. Cáceres, P. Lukáč, A. Blake, Phil. Mag. 88 (2008) 991–1003.
[24] S.R. Agnew, D.W. Brown, C.N. Tomé, Acta Mater. 54 (2006) 4841–4852.
[25] D.L. Yin, J.T. Wang, J.Q. Liu, X. Zhao, J. Alloys Compd. 478 (2009) 789–795.
[26] D.V. Wilson, J.A. Chapman, Philos. Mag. 8 (1963) 1543–1551.
[27] A. Jain, O. Duygulu, D.W. Brown, C.N. Tome, S.R. Agnew, Mater. Sci. Eng. A Struct. Mater. 486 (2008) 545–555.
[28] W.J. Kim, C.W. An, Y.S. Kim, S.I. Hong, Scr. Mater. 47 (2002) 39–44.
[29] A.J. Ardell, Metall. Mater. Trans. A 16 (1985) 2131–2165.